

A STUDY OF STRESS IN DEVONIAN SHALES OF THE APPALACHIAN PLATEAU

Final Technical Report

By

K.F. Evans and T. Engelder

July 1987

Submitted to:

U.S. Department of Energy
Office of Fossil Energy,
Morgantown Energy Technology Center,
Morgantown, West Virginia

Work Performed Under Contract No.: DE-AC21-83MC20337

and also submitted to contributing parties:

Schlumberger-Doll Research Division of Schlumberger Technology
Corporation,
Old Quarry Rd.,
Ridgefield, Connecticut.

Exxon Production Research
PO Box 2189,
Houston, Texas

DISCLAIMER

"This report was prepared as an account of work sponsored by an agency of the United States Government. Neither the United States Government nor any agency thereof, nor any of their employees, makes any warranty, express or implied, or assumes any legal liability or responsibility for the accuracy, completeness, or usefulness of any information, apparatus, product, or process disclosed, or represents that its use would not infringe privately owned rights. Reference herein to any specific commercial product, process, or service by trade name, trademark, manufacturer, or otherwise, does not necessarily constitute or imply its endorsement, recommendation, or favoring by the United States Government or any agency thereof. The views and opinions of authors expressed herein do not necessarily state or reflect those of the United States Government or any agency thereof."

A STUDY OF STRESS IN DEVONIAN SHALES

OF THE APPALACHIAN PLATEAU

Prepared by:

K.F. Evans and T. Engelder,
Lamont-Doherty Geological Observatory of Columbia University
Palisades, New York.

ABSTRACT

Examination of available data shows that the state-of-stress in the Paleozoic sediments of the Appalachian Basin is dominated by NE-ENE compression, as is found over much of the Eastern US west of the Appalachian highlands. Locally, there is a tendency for maximum stress orientation to parallel the structural trend of the basin. An Upper Silurian salt decollement extends southward from the Lakeshore region of Western New York and Ohio to northern West Virginia. Examination of commercial hydrofracture records in the northern and western parts of this region suggests that mechanical decoupling at the salt horizon has permitted different stress levels to develop in the overlying and underlying sections. Stress ratios, which express the least horizontal stress as a fraction of the overburden at the depth of the measurement, are found to approach or exceed unity in Devonian and younger sands and shales. In contrast stress ratios determined in the underlying Silurian and older sediments range between 0.5 - 0.7. The magnitude of the NE-ENE maximum horizontal stress in the Devonian section from the few measurements available suggest it is significantly greater than the least horizontal stress.

The detailed pattern of stress within strata of the Devonian section was investigated by performing 78 stress measurements to 1 km depth in three boreholes a kilometer or so apart near S. Canisteo NY. The stratigraphic section tested extended from the Dunkirk shale to the Moscow shale, and contains several thin (5-17m) sand-rich beds near the base of the Rhinestreet shale, and the Tully limestone. The dominant component of horizontal stress throughout the section was found to be ENE compression. The sandstone and Tully limestone beds were found to host higher stresses than the surrounding shales which is ascribed to their greater stiffness as determined from sonic and density logs. Thus, stress contrasts between beds of substantially different lithology are largely the result of elastic shortening of the section in response to NE contemporary compression.

Anomalously low stresses were found in all shales below the base of the Rhinestreet. The decline in shale stress is first apparent in the lowermost 100m of the Rhinestreet which contains three sand beds, but the principal drop occurs at the lowermost bed known locally as the Grimes sandstone. Immediately below this bed, the stress ratio drops to as low as 0.67. This decline in shale stress contrasts strongly with the high stresses measured in the sands and the Tully limestone. It does not correlate with any systematic variation in elastic constants for the shale as determined from the sonic logs and hence cannot be explained in terms of elastic shortening of relatively compliant beds. However, it correlates with undercompaction of shales determined from chlorite fabric analyses performed on core samples from a nearby well. Similar analyses performed on outcrop samples taken from the region together with joint propagation data suggest that the shales below the Rhinestreet base developed abnormally high pore-pressures during Alleghanian tectonism. This, together with the Alleghanian shortening estimates derived from the chlorite fabric analysis of core, and observations of crinoid distortion suggest that the mechanical response of the sections above and below the Rhinestreet base to Alleghanian

compression was different, due in large part to restricted fluid circulation in the lower section. The anomalously low stress zone is explained in terms of remnant stresses derived from the different responses.

Thus, stresses in the Devonian rocks of the northern Appalachian basin are dominated by ENE oriented compressive stress of contemporary tectonic origin. Stress contrasts between adjacent beds are thus determined largely by stiffness contrasts which can be measured using full-waveform sonic logs. Departures from this general characterisation exist, however, and may be related to overpressuring of the shales below the Rhinestreet base during Alleghanian time. Further stress measurements are needed to determine whether the anomalously low stresses measured in shales below the Rhinestreet is a local phenomenon, or whether it is widespread.

Acknowledgements

This work was funded in greatest single part by USDOE under contract DE-AC21-83MC20337. Substantial contributory funding was also provided by Exxon Production Research (EPR), Lamont-Doherty Geological Observatory (L-DGO) and Schlumberger-Doll Research (SDR). We thank C. Komar (DOE), L. Lacy (EPR), R. Plumb (SDR), C. B. Raleigh (L-DGO), and C. Shaunessy (EPR) for their vital support in obtaining these funds.

We gratefully acknowledge those individuals who, by sharing their unpublished data or donating their services free of charge, contributed substantially to this work. We specifically thank R. Beardsley (Columbia Natural Resources), D. Copeley (Berea Oil and Gas), G. Oertel (University of California at Los Angeles), and A. M. Van Tyne (Van Tyne Consulting). We also acknowledge the co-operation of D. Phillips and Vandermark Associates in granting permission to use their wells.

All borehole televiwers used in this project were loaned from a division of the Ocean Drilling Project based at L-DGO. We thank D. Moos and R. Anderson for co-operation.

We thank the Technical Project Officer at METC, A. Yost II, for his patient co-operation which allowed us to fully synthesize the data.

Finally we thank the graduate students and technical staff of L-DGO and Pennsylvania State University for support in the laboratory and the field. These include P. Barnes, G. Boitnott, I. Meglis, C. Rine, and T. Koczynski.

TABLE OF CONTENTS

TITLE PAGE.....	i
ABSTRACT.....	ii
ACKNOWLEDGEMENT.....	iv
TABLE OF CONTENTS.....	v
LIST OF TABLES.....	viii
LIST OF FIGURES.....	ix
EXECUTIVE SUMMARY.....	1
INTRODUCTION.....	5
SECTION 1:	<u>Investigations of the Mechanical Behavior of Two Common Straddle-Packer Designs</u>
1.1	Objective..... 8
1.2	Background..... 8
1.3	Experimental Method
1.3.1	Simulator Design..... 10
1.3.2	Calibration..... 12
1.3.3	Theory..... 12
1.3.4	Test Procedure..... 15
1.4	Results
1.4.1	7.2 cm Straddle System with Rigid Packer Coupling.... 17
1.4.2	17.8 cm Straddle System with Sliding Packer Coupling 22
1.5	Discussion..... 27
1.6	Conclusions..... 34
SECTION 2:	<u>Geological Background and Regional Stress Character</u>
2.1	Objective..... 35
2.2	Basin History and Structure
2.2.1	Basin History..... 35
2.2.2	Structure..... 38
2.3	Regional Contemporary Stress Survey
2.3.1	Orientation of Maximum Horizontal Principal Stress..... 40
2.3.2	Horizontal Stress Magnitude and Stress Ratio..... 42
2.4	Discussion..... 47
2.5	Conclusions..... 49
SECTION 3:	<u>Detailed 3-D Mapping of Stress in Devonian Shale at S.Canistoto, NY : Measurements and Technique</u>
3.1	Objective..... 51

3.2	Location, Stratigraphy and Structure of the Study Area	
3.2.1	Location.....	51
3.2.2	Stratigraphy.....	51
3.2.3	Structure.....	55
3.3	Instrumentation.....	56
3.4	Field Project Design.....	56
3.4.1	Stress Measurement Technique.....	59
3.4.2	Size of Induced Fractures.....	61
3.5	Results.....	63
3.5.1	Instantaneous Shut-in Pressures.....	63
3.5.2	The Effects of Topographic Loading on In-Situ Stresses.....	67
3.5.3	Minimum Horizontal Principal Stress Magnitude.....	70
3.5.4	Maximum Principal Horizontal Stress.....	71
3.5.5	Stress Estimates and the Bulk Shear Strength of Devonian Shale.....	77
3.5.6	Fracture Trace Geometry.....	78
3.5.7	The Effects of Fracture Propagation around the Packer Seats.....	79
3.6	Discussion.....	82
3.7	Conclusions.....	84
SECTION 4:	<u>S. Canisteo Stress Data: Interpretation and Supportive Geophysical Studies</u>	
4.1	Objective.....	86
4.2	Canisteo Stress Data and the Regional State of Stress	
4.2.1	Summary of Regional Stress.....	86
4.2.2	Relation between Local Stress at S. Canisteo and Regional Stress.....	86
4.2.3	The Effects of Material Property Contrasts.....	89
4.3	Core Studies Overview.....	94
4.3.1	Thin section analysis of Samples from the Vicinity of the Grimes Sandstone.....	95
4.4	Total Strain Measurements on NY1 Core Samples	
4.4.1	X-Ray Pole-figure Goniometer Measurements on Core from NY1.....	95
4.4.2	Results of Chlorite Fabric Analysis on NY1 Core Samples.....	97
4.4.3	Overpressure Development and Models for Alleghanian Deformation.....	101
4.5	The Nature of the Sub-Rhinestreet Stress Anomaly.....	103
4.6	Chlorite Fabric and the Mechanical Anisotropy of Devonian shales.....	107
4.7	Conclusions.....	109
REFERENCES.....		110
APPENDIX 1 :	Regional Stress Data Indexes.....	118

A1.1	Index to Stress Orientation Map.....	119
A1.2	Explanation to Stress Ratio Maps.....	121
A1.2.1	Index to Stress Ratio Map for Devonian & Younger Rocks.....	122
A1.2.2	Index to Stress Ratio Map for Silurian and Older Rocks.....	126
APPENDIX 2 :	S. Canisteo Stress Measurement Data Tables.....	130
A2.1	Explanation of Data Table Headings and Suffixes.....	131
A2.1.1	Tabulated Summary of Stress Tests in the Wilkins Well.....	132
A2.1.2	Tabulated Summary of Stress Tests in Appleton Well.....	134
A2.1.3	Tabulated Summary of Stress Tests in O'Dell Well.....	135
APPENDIX 3 :	Induced Fracture Trace Geometry.....	136
A3.1.1	Tabulated Summary of Image Traces in the Wilkins Well.....	137
A3.1.2	Sketches of Image Traces observed in the Wilkins Well.....	138
A3.2	Sketches of Image Traces Observed in the Appleton Well ...	139
APPENDIX 4 :	Shale Material Properties and the Sub-Rhinestreet Stress Anomaly	146
A4.1	Summary of Poisson's Ratio values for Devonian Shales ...	147
A4.2	Summary of Young's Modulus for Devonian Shales	147
A4.3	Estimation of modulus contrast required to explain the low stress anomaly below the K-sand	147

SECTION 1

INVESTIGATIONS OF THE MECHANICAL BEHAVIOR OF TWO COMMON STRADDLE-PACKER DESIGNS

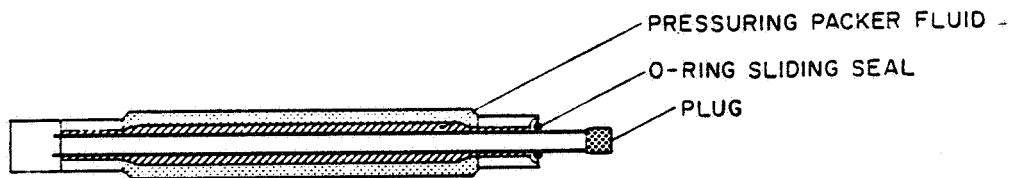
1.1 OBJECTIVE

To evaluate the mechanical behavior and sealing characteristics of two common straddle packer designs under conditions which replicate those encountered during hydraulic fracturing, to identify aspects of design which promote efficient behavior, and to acquire a straddle packer system well suited for wireline stress measurements in Devonian shale.

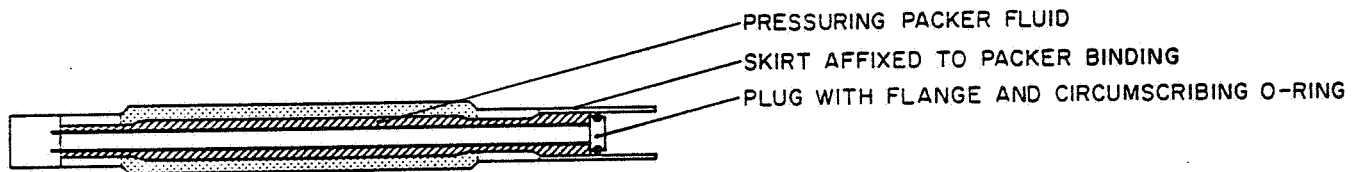
1.2 BACKGROUND

The study was originally motivated by observations that arose during a series of stress measurements conducted in a 1 km deep 7.6cm diameter borehole penetrating granite near the town of N. Conway, NH (Evans et al., 1987). An objective of this field campaign was to field test of the wireline 'microfrac' system we intended to field in the Appalachian basin project. During these tests we occasionally observed what appeared to be leakage of fluid past the packer seals at pressures significantly lower than the initial packer setting pressure even though it was clear that no fracture was present. This unwelcome behavior was certainly not anticipated or understood. Very few experimental studies of straddle packer behavior have been published and none provided an explanation of this behavior. As the breakdown pressures we expected to encounter during the Canisteo stress measurement program exceeded those in the field tests, we developed a laboratory-based 8.6cm ID borehole simulator to investigate the cause of the low-pressure flow-by. The simulator was constructed from a length of heavy-duty steel casing which was instrumented with strain gages. From the measured strains it was possible to estimate the stresses which the packers were applying to the casing during pressurization. The straddle-packer assembly used in the measurements utilized a rigid coupling between the packers within the interval. A schematic representation of the rigid-coupling straddle configuration is shown in Figure 1.1c.

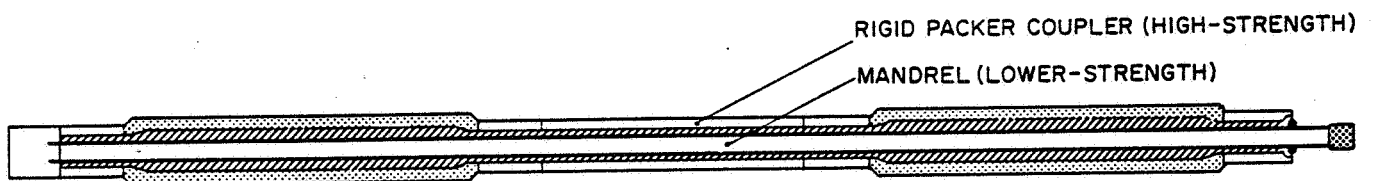
Based upon the results of the investigation, a straddle packer design was selected for use in the 20 cm diameter S. Canisteo boreholes. The mechanical configuration of this tool was quite different to that used in the N. Conway tests. In contrast to the former, this system utilized a free-sliding coupling between the packers within the interval (Figure 1.1d), a design which might be expected to behave differently from the rigidly-coupled configuration. The packer elements which featured in the 17.8cm system were also much stiffer (axially) than those in the 7.2cm system. Prior to fielding the new system a 20.3cm ID simulator was constructed to evaluate the new design and the results showed that the selected system behaved in almost an ideal manner. This was born out by fieldwork operation during which differential pressures across the packer seals of 44 MPa were attained without leakage, even though the packers were originally set a mere 5 MPa above hydrostatic pressure.



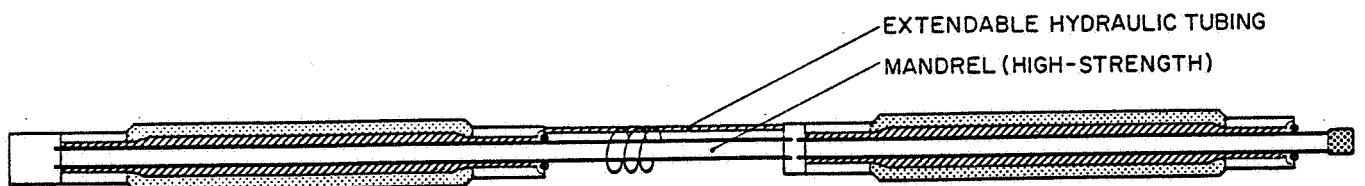
a) SINGLE PACKER ON MANDREL



b) SINGLE PACKER ON MANDREL FITTED WITH PRESSURE SKIRT LOWER SEAL



c) STRADDLE SYSTEM WITH RIGID COUPLING OF PACKER IN INTERVAL



d) STRADDLE SYSTEM WITH SLIDING COUPLING OF PACKER IN INTERVAL

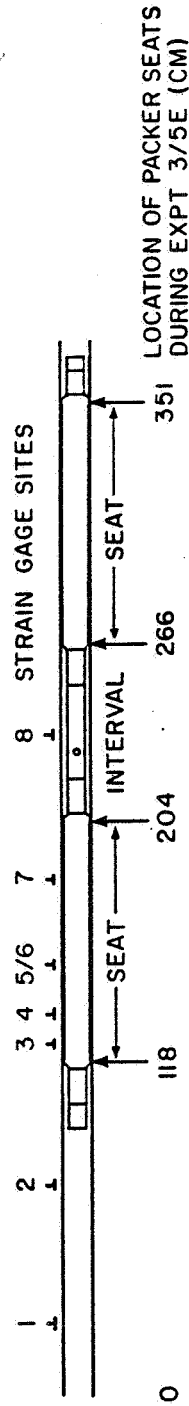
Figure 1.1; Schematic representation of the mechanical configurations of the three packer systems tested. Note that in 'c' (the rigidly-coupled system) the mandrel serves only as an O-ring sealing surface and does not support the pull-apart force developed between the packers as does the mandrel in illustration 'd'.

It is important from the outset to clarify terminology. We shall refer to fluid pressure within a straddled interval as 'Interval Pressure', P_I , to fluid pressure within a packer element as 'Packer Pressure', P_P , and to the pressure which a packer element exerts against the internal wall of a borehole or casing as 'Seal Pressure', P_S . The ratio of seal pressure to packer pressure will be referred to as 'Seal Efficiency', S_E , and the ratio of an incremental increase in seal pressure to the corresponding increase in packer pressure will be called 'Incremental Seal Efficiency', $dS_E (= dP_S/dP_P)$. It will also prove useful to define some measure of the efficiency by which changes in interval pressure give rise to changes in packer pressure. We shall call the ratio dP_P/dP_I the 'Incremental Coupling Efficiency'. It should be noted that all incremental quantities are in practice calculated over 2.5MPa pressure steps and will in general vary as pressures change.

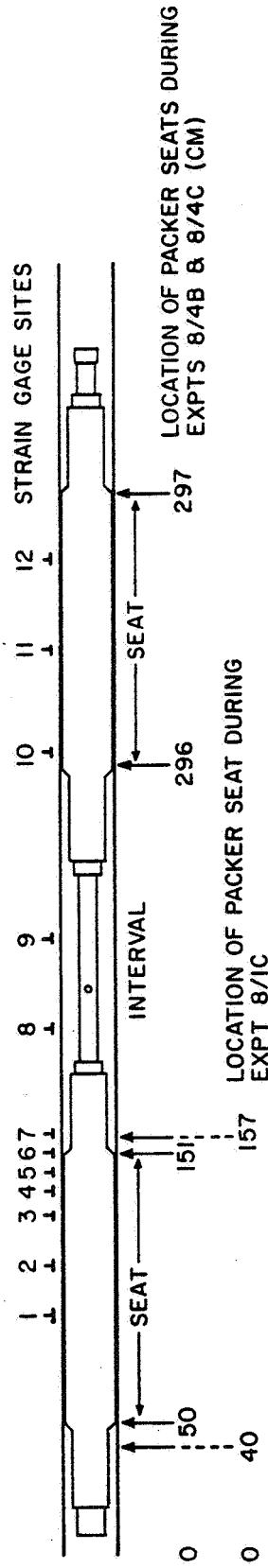
1.3 EXPERIMENTAL METHOD

1.3.1 Simulator Design:

Both borehole simulators consisted of a length of 'black-pipe' casing of appropriate internal diameter for the tool to be tested. Wall thickness was chosen to permit safe internal pressurization over the desired pressure range which, for practical reasons, we limited to 25 MPa. Radial and circumferential precision strain gauges (Micro-Measurements type EA-06-125TF-120) were then affixed in pairs at a number of carefully chosen sites along the casing taking care to avoid (as much as possible) surface pits in the steel. Site distribution was chosen to best reveal the pattern of strain imposed to the casing by pressurization of the specific straddle tool in question. The locations of the gauge sites for the 8 cm and 20 cm simulators is shown in Figure 1.2a and 1.2b respectively. Also shown is the position of the straddle tools within the respective casings for the specific tests we have chosen to discuss. The casings were supported horizontally. Interval and packer pressure were both monitored continuously throughout the tests using two Sensotec Model TJE transducers (precision of 1 part in 1000) each having a range of 69 MPa. The resistance of each strain gauge was monitored in one of two ways: either indirectly but continuously using a Wheatstone bridge and strip chart recorder, or directly but discretely using a HP3421A multiplexed data logger programmed for 4-wire resistance measurement in a data loop containing a printer and cassette recorder. The data logger was programmed to poll each of ten resistance channels every minute for the duration of the experiment. Resolution of each sample was equivalent to about 4 microstrain. Although the data logger was certainly convenient, the Wheatstone bridge system of recording was preferred as it provided a continuous record of strains at the gauge sites and had intrinsically superior resolution. A total of eight gauges (four sites) were monitored continuously in this manner.



a) 8.6 CM BOREHOLE SIMULATOR: TOOL SHOWN IN POSITION AS FOR EXPT 3/5E.



b) 20.3 CM BOREHOLE SIMULATOR: TOOL SHOWN IN POSITION AS FOR EXPTS 8/4B & 8/4C.



Figure 1.2; Location of strain gauge pairs affixed to simulator casings and the position of the packers within the casings during the various experiments discussed in the text.

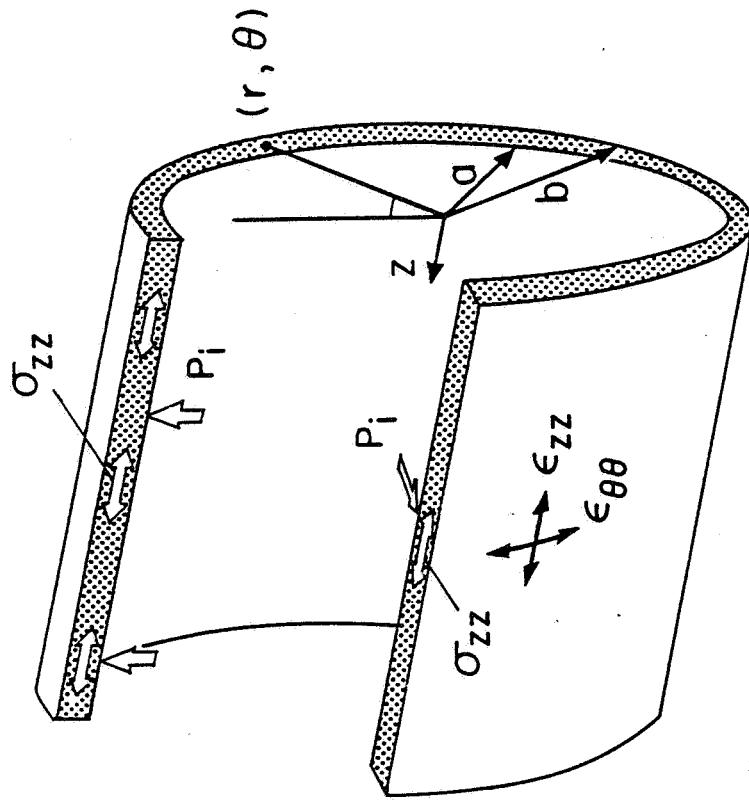
1.3.2 Calibration:

A critically important element of the experiment was to calibrate the gauges in terms of their actual response to internal pressure within the casing. It is possible to calculate quite precisely the theoretical response of the gauge to stresses applied to the inside wall of the casing by adopting the manufacturer's supplied gauge factor and applying the stress-strain relations appropriate for an internally pressurized cylinder. However, in practice the method proved too imprecise. There were several reasons for this: firstly, the elastic modulus of the casing steel was not known to adequate precision; secondly, the somewhat coarse method of manufacturing the 'black-pipe' resulted in variations in surface strain (in response to uniform stress) on the scale of the gauge lengths (2 cm); and finally, surface roughness made coupling potentially imperfect. To circumvent these problems, each gauge pair was calibrated by positioning the straddle tool in the casing such that the pair in question lay well within the interval. After setting the packers, the interval pressure was raised a known amount and the response of the gauges noted. The predicted internal pressure at each gauge site could then be computed (applying the relations derived in the following section) using a value of Young's modulus for the steel which minimized the discrepancy between predicted and known internal pressures summed over all sites. A multiplicative strain correction factor was then calculated for each site which when applied to the measured circumferential strain yielded an estimate of internal pressure which agreed with the calibrating pressure. Only the 'circumferential strain' gauges were calibrated in this manner. Calibration of the axial gauges would have required a precisely known axial load to be applied to the casing. This additional task was considered unnecessary as we were primarily interested in resolving internal casing pressures from the observed strains and for this, the circumferential gauges were essentially an order of magnitude more important. Thus, axial gauge strains were taken on face value; that is, they were not corrected for the effects of strain field heterogeneity. Consideration of the correction factors deduced for the circumferential gauges suggest the error is less than 5%.

1.3.3 Theory:

In order to interpret the strains $\epsilon_{\theta\theta}$ and ϵ_{zz} observed at a given site in terms of the causative stresses, P_i , the internal pressure, and σ_{zz} , the axial stress, which act on the casing at that site, we shall assume that locally there are no axial gradients in either stress or strain. This is shown schematically in Figure 1.3. Clearly the assumption is not valid near the ends of the packer seats where large gradients in applied internal pressure exist and give rise to bottle-neck deformation of the casing with attendant 'cylindrical' bending stresses and strains. However, provided the site is more than a casing diameter away from the end of a packer seal, we consider the assumption to be generally valid. The casing is considered to be a regular linear-elastic cylinder of internal diameter, a , and external diameter, b , having a Poisson's ratio, ν , and Young's modulus, E . Compression is taken as positive.

Jaeger and Cook (1976 ,p 135) have derived the equations which describe the stresses and strains developed in an internally pressurized cylinder under plane strain conditions. For our purposes it is necessary to generalize these relations to permit an



COMPRESSION POSITIVE

INTERNALLY PRESSURED CYLINDER WITH UNIFORM AXIAL STRAIN.
 (ALL STRESS AND STRAIN COMPONENTS INDEPENDENT OF Z)

Figure 1.3: Co-ordinate system and stress components considered in the analysis.

arbitrary axial stress, σ_{zz} , to exist in the cylinder along with the internal pressure, P_i , both of which are independent of the 'r' and 'z' co-ordinates (Figure 1.3). The modified equations do not differ greatly from the plane strain case and are,

$$\sigma_{rr} = -\frac{a^2}{(b^2 - a^2)} P_i + \frac{a^2 b^2}{r^2 (b^2 - a^2)} P_i \quad , \quad (1.1)$$

$$\sigma_{\theta\theta} = -\frac{a^2}{(b^2 - a^2)} P_i - \frac{a^2 b^2}{r^2 (b^2 - a^2)} P_i \quad , \quad (1.2)$$

$$\text{hence } \sigma_{rr} + \sigma_{\theta\theta} = -\frac{2 a^2}{(b^2 - a^2)} P_i \quad , \quad (1.3)$$

$$\sigma_{zz} = \nu (\sigma_{rr} + \sigma_{\theta\theta}) + E \epsilon_{zz} \quad , \quad (1.4)$$

$$= -\frac{2 \nu a^2}{(b^2 - a^2)} P_i + E \epsilon_{zz} \quad , \quad (1.5)$$

where $b \geq r \geq a$.

Evaluating equations (1.1) and (1.2) at the external surface of the casing, $r = b$, gives,

$$\sigma_{rr} |_{r=b} = 0 \quad ,$$

$$\sigma_{\theta\theta} |_{r=b} = -\frac{2a^2}{(b^2 - a^2)} P_i \quad . \quad (1.6)$$

The stress-strain relations for the case of uniform axial strain are again given in Jaeger and Cook (1976, p. 115) and are,

$$\epsilon_{rr} = \frac{1}{E} \{ (1 - \nu^2) \sigma_{rr} - \nu(1 + \nu) \sigma_{\theta\theta} \} - \nu \epsilon_{zz} \quad , \quad (1.7)$$

$$\epsilon_{\theta\theta} = \frac{1}{E} \{ (1 - \nu^2) \sigma_{\theta\theta} - \nu(1 + \nu) \sigma_{rr} \} - \nu \epsilon_{zz} \quad . \quad (1.8)$$